Activating ZnO nanorods photoanodes in visible light by CdS surface sensitiser

Indranil Biswas, Piyali Roy (Kundu), Prasanta Kumar Sinha, Moumita Kanu, Ashim Kumar Chakraborty ✉

Material Characterization and Instrumentation Division, CSIR-Central Glass and Ceramic Research Institute, Jadavpur, Kolkata-700032, India
✉ *E-mail: ashim3121@gmail.com*

Published in Micro & Nano Letters; Received on 16th November 2018; Revised on 18th March 2019; Accepted on 5th April 2019

Thin films of *c*-axis aligned uniform ZnO nanorods (NRs) were fabricated on to fluorine-doped tin oxide-coated soda lime glass substrate by a two-step chemical route. Thereafter ZnO NRs/CdS core shell structures were successfully synthesised by depositing CdS layer on top of vertically aligned ZnO NRs using less hazardous nanocrystal layer deposition technique. The presence of CdS in ZnO NRs/CdS core shell structures was confirmed by energy dispersive X-ray analysis. Examination of structure and morphology of the fabricated films by X-ray diffraction (XRD) and field emission scanning electron microscopy (FESEM) revealed that both films have one-dimensional hexagonal wurtzite structure. Optical properties evaluated from ultraviolet–visible and photoluminescence spectra demonstrated better photo response of ZnO NRs/CdS core shell structure with respect to bare ZnO NR structure. Optical to chemical conversion efficiency of ZnO NRs/CdS photoanode was found to be ∼1.75 times higher than bare ZnO NRs photoanode in photo electrochemical water splitting under visible light.

1. Introduction: In the present decade, development of nanostructured materials with core/shell type structure is drawing interest in the field of photovoltaic, photo electrochemical (PEC), optoelectronic, biological and chemical applications [1, 2]. PEC processes are presently being used in the conversion of clean and earth abundant solar energy to storable chemical energy. ZnO is being extensively studied as a semiconductor photoelectrode material for PEC water splitting due to its low cost, wide band gap, non-toxicity, high electron mobility and high mechanical and thermal stability [3, 4]. However, a very small percentage of light [mainly ultraviolet (UV)] present in the solar spectrum can be absorbed and utilised by ZnO due to its wide band gap of ∼3.37 eV. To exploit the visible region of the solar spectrum, various narrowband gap semiconductors such as CdS, CdTe, CdSe, PbS, and PbSe are used as sensitising materials with large band gap ZnO [2, 5–7] for increasing its efficiency during PEC water splitting. Among them, CdS can be the semiconductor of choice for sensitising ZnO due to well visible light harvesting capability, high abundance and low production cost [2, 5–16]. The similarity in the crystal structure, congruousness in band alignment and wide spectrum utilisation make CdS compatible to ZnO to construct efficient core/shell type heterostructure composite which results in increased photo-generated charge carriers and their separation [7]. CdS have a higher electron affinity than ZnO. According to Anderson's model, between CdS and ZnO a type II heterostructure is formed. As the visible light is radiated on the ZnO nanorods (NRs)/CdS composite, the electron is generated in the conduction band of CdS and it jumps to the conduction band of ZnO by ballistic diffusion [17]. The time required for an electron to be transferred from the conduction band of CdS to the conduction band of ZnO is about 18 ps, which is less than the lifetime of an electron in CdS [18]. Hence, it is expected that high PEC conversion efficiency can be achieved when ZnO NRs sensitised with CdS are used as photoelectrodes.

In the present study, synthesis and characterisation of one-dimensional (1D) ZnO NRs & ZnO NRs/CdS core shell structures are reported. After a detailed structural and morphological examination, the optical properties are correlated with PEC properties. From experimental results, it was observed that the ZnO NRs/CdS core shell shows better photo response and high PEC activity in the visible region than bare ZnO NRs. The mechanism behind the improved optical and PEC properties of ZnO NRs/CdS core shell in the visible region is also discussed.

2. Experimental

2.1 Chemicals: All reagents were of analytical grade and purchased from Sigma-Aldrich and Merck. Potassium nitrate (KNO_3, 98%), zinc acetate di-hydrate [$Zn(CH_3COO)_2{\cdot}2H_2O$, 99%], di-ethanolamine ($C_4H_{11}NO_3$, 99%), isopropanol (C_3H_8O, 99%), cadmium sulphate ($CdSO_4$, 99%), nitric acid (HNO_3, 70%) and thioacetamide (C_2H_5NS, 99%) were used.

2.2 Preparation of ZnO NRs: ZnO NRs were deposited on fluorine-doped tin oxide (FTO)-coated soda lime glass (SLG) substrate (Techinstro, sheet resistance 15Ω/□) using spin coating followed by electro chemical deposition technique. Spin coating was used at 1500 rpm for 30 s to deposit ZnO seed layer using the precursor solution which was prepared by adding 0.5 M Zn $(CH_3COO)_2$ and 0.5 M di-ethanolamine in isopropanol [19]. The coated sample was dried on a preheated hot plate at 180°C for 10 min. The process of coating and drying was repeated five times to obtain the desired thickness of the seed layer. The prepared seed layer was then thermally treated in air at 400°C for 60 min.

Electrochemical deposition of ZnO NRs was carried out on to ZnO seed layer in the chronoamperometric mode with $V_{WE/CE} = -1.1$ V for 15 min at a temperature of 80°C using Metrohm Autolab PGSTAT302N electrochemical workstation. The seed layer coated FTO substrate was used as the working electrode (WE) while a 99.9% pure zinc plate (Alfa Aesar) was used as the counter electrode (CE). For deposition of pure ZnO film, an aqueous precursor solution of 50 mM Zn $(CH3COO)_2$ and 0.1 M KNO_3 was used. The pH of the precursor solution was adjusted to ∼5.8 using 2 mM HNO_3 [20]. The electrodeposition potential was predetermined using linear sweep voltammetry (LSV) performed in the precursor solution. The as-deposited films were washed with distilled water and air dried at room temperature and placed for annealing at 400°C for 60 min in the air. Uniform and well adhered pure ZnO film was found to be deposited on the seed layer.

2.3 Deposition of CdS layer: CdS buffer layer was coated on the surfaces of the prepared ZnO NRs using nanocrystal layer

deposition (NCLD) technique [19, 21]. An aqueous precursor solution containing 20 mM $CdSO_4$ and 20 mM thioacetamide were mixed and sonicated for 10 min. ZnO NRs deposited on FTO substrate were placed in the solution for 60 min at room temperature. Once deposition was complete, the colour of the transparent substrate became yellow. The as-deposited samples were thoroughly cleaned with deionised water and dried in air. Finally, the as-prepared FTO/ZnO/CdS samples were annealed in air at 350°C for 30 min. The various steps needed for the formation of ZnO NRs/CdS core shell is schematically shown in Fig. 1 and the photo of the deposited thin film is shown in Fig. 2

The NCLD technique is a modified chemical bath deposition (CBD) approach that enables selective deposition on to ZnO NRs only. Being an amphoteric compound, ZnO easily suffers from leaching under both low and high pH conditions at the (002) facet which has low surface energy [21]. So the pH of NCLD precursor solution was kept near ∼6.6 in order to minimise the possibility of etching of ZnO surface.

2.4 Thin film characterisation: X-ray diffraction (XRD) studies were carried out for phase identification using a Bruker D8 Advance Davinci XRD System with Cu Kα radiation ($\lambda = 1.54$Å, 1.6 kW, 40 mA, scan rate = 0.05°/s, $2\theta = 20°$–$80°$). The morphological properties of the ZnO NRs and ZnO NRs/CdS core shell were studied using a ZEISS (SIGMA) field emission scanning electron microscope (FESEM). For this study, the sample was prepared by giving a coating of a thin layer of graphite using high vacuum evaporation (carbon evaporator, make: Edwards (UK)) to avoid charging effect and to improve the signal-to-noise ratio. The energy dispersive X-ray (EDX) analysis of ZnO NRs/CdS core shell was carried out using EDAX model X-Max manufactured by Oxford instrument (UK). The UV–visible (Vis) optical absorption spectrum was recorded on a Shimadzu UV3600PC UV–Vis–near-infrared spectrophotometer and photoluminescence (PL) spectrum was measured by a Perkin Elmer LS55 spectrophotometer using an excitation wavelength of 350 nm at room temperature. For investigation of PEC behaviour, ZnO NRs and ZnO NRs/CdS shell photoanodes were used as a working electrode (WE), Pt wire was used as a counter electrode (CE) and Ag/AgCl/3 M KCl was used as a reference electrode. 0.5 M Na_2SO_4 was used as the electrolyte. Electrochemical work station (Metrohm Autolab PGSTAT302N), a 150 W Xenon Arc Lamp with illumination intensity of 100 mW cm^{-2} (AM1.5), a 420 nm glass filter (used to block UV light), a quartz wafer filter (used to remove infrared radiation >800 nm) and a light chopper unit were employed for chronoamperometry (j–t) and linear sweep voltammetry (j–v) experiments. The overall transmittance (T) for visible light illuminating the photoanode was 0.8.

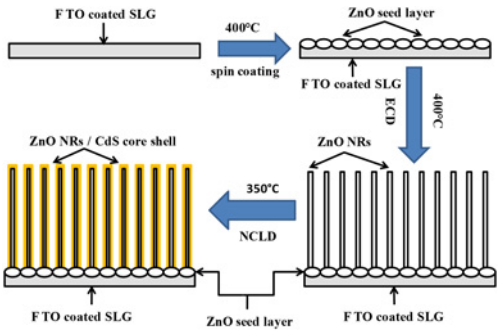

Fig. 1 *Schematic representation of the formation of ZnO NRs/CdS core shell thin film*

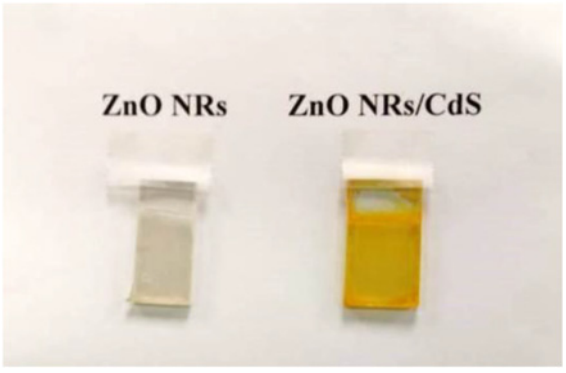

Fig. 2 *Optical image of fabricated thin films*

3. Results and discussion

3.1 Structure and morphology: The phase and crystal structure of the prepared thin films were confirmed by XRD analysis (Fig. 3). Prior to CdS deposition, one main peak corresponding to ZnO (002) was confirmed at 34.4548°. Unit cell parameters $a = 3.253$ Å and $c = 5.206$ Å are calculated using the lattice equation of the wurtzite structure (1) [22]

$$a = d_{hkl}\sqrt{\frac{4}{3}\left(h^2 + hk + k^2\right) + l^2\left(\frac{a}{c}\right)^2}, \quad (1)$$

where h, k, *and* l are miller indices and d_{hkl} is the interplanar distance. The calculated values of a and c agreed well with the ICDD pdf card no. 01-082-8987. The intense (002) ZnO diffraction peak confirmed that the ZnO NRs were highly crystalline with a hexagonal wurtzite structure. In addition, the preferential growth of the ZnO NRs was perpendicular to the substrate, which was confirmed by FESEM images shown in Fig. 4*a*. Since ZnO NRs were single crystals with c-axis aligned along their longitudinal axis, the degree of crystallographic orientation indicated the verticality of the NRs (1D). The results confirmed that ZnO NRs were well-shaped c-axis oriented hexagonal columns and improvement of these characteristics is attributed to the use of ZnO seed layer [23]. The remaining weak diffraction peaks were observed and positioned at 31.7596°, 36.2516°, 47.5481°, 56.5576°, 62.8625°, 65.4727°, 67.9053° and 72.6534° corresponding to 100, 101, 102, 110, 103, 200, 112 and 004 reflecting planes of ZnO crystallites, respectively.

The CdS layer deposited by NCLD was not observed from XRD analysis. This might be due to the smaller amount of CdS nanocrystal deposition on the surface of ZnO NRs [19].

FESEM images were obtained to study the surface morphology of the prepared ZnO NRs and ZnO NRs/CdS core shell thin films. The top view of FESEM micrograph of ZnO NRs (Fig. 4*a*) shows a compact hexagonal wurtzite surface morphology with dense and uniform hexagonal NRs along the c-axis (1D). The

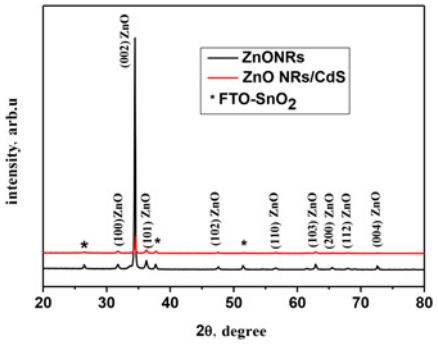

Fig. 3 *XRD pattern of bare ZnO NR and ZnO NRs/CdS core shell thin films*

doi: 10.1049/mnl.2018.5700

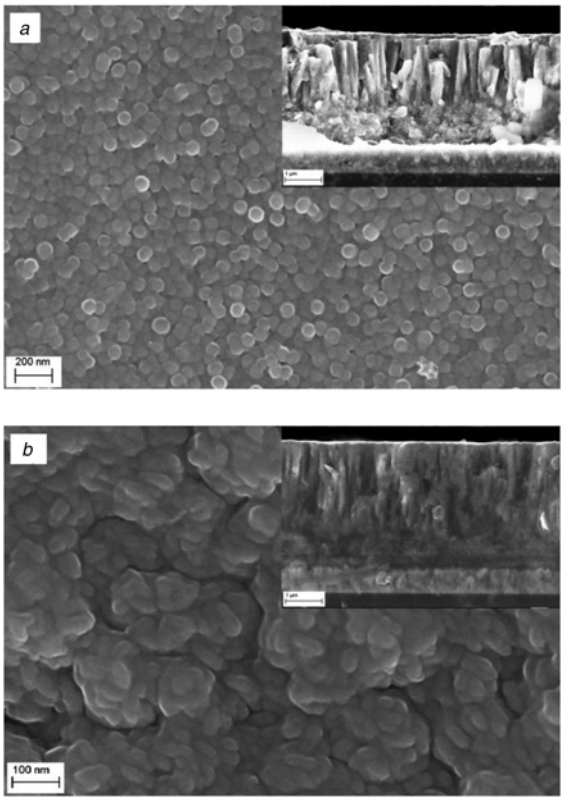

Fig. 4 *FESEM images of*
a ZnO NRs, (inset) cross-sectional view
b ZnO NRs/CdS core shell, (inset) cross-sectional view

diameters of the ZnO NRs are ~50 nm. From the cross-sectional view (Fig. 4*a* inset) of the ZnO NRs, it is observed that the lengths of the ZnO NRs are ~2 µm. The top view of the FESEM micrograph of ZnO NRs/CdS shell (Fig. 4*b*) depicts that CdS nanoparticles are embedded into the surface of ZnO NRs forming a uniform cell layer. The cross-sectional view of ZnO NRs/CdS shell (Fig. 4*b* inset) further shows that the length and diameter of ZnO NRs are not affected due to CdS shell layer deposition.

EDX analysis of ZnO NRs/CdS core shell was carried out to analyse the chemical composition. The EDX spectrum in Fig. 5 shows the elemental composition, which confirms the presence of Zn, O, Cd, and S.

3.2 Optical properties: From the UV–Vis absorption spectrum of bare ZnO NRs (Fig. 6) thin films, it is observed that the films are a good absorber of UV light. From the absorption spectra of ZnO NRs/CdS core shell nanostructure, it has been observed that there is a considerable increase in absorbance in the visible region after coating with a CdS shell layer. The absorption edge of bare ZnO NRs at 391 nm is red shifted to 523 nm after the coating, thus

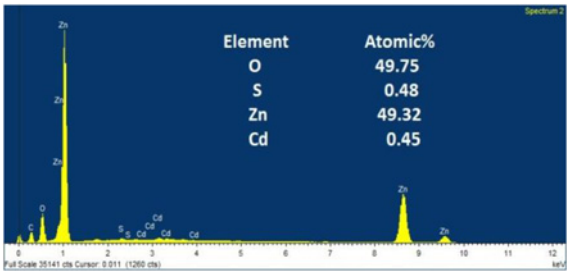

Fig. 5 *EDX spectrum of ZnO NRs/CdS core shell thin film*

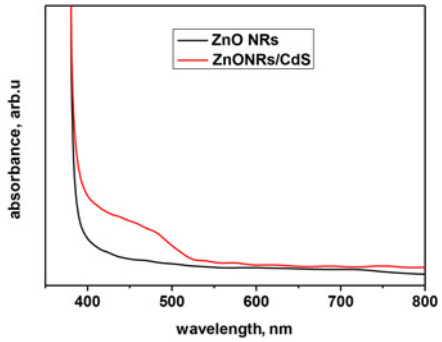

Fig. 6 *UV–Vis absorption spectra of ZnO NRs and ZnO NRs/CdS core shell nanostructure*

covering most of the visible region. This is one of the most important reasons behind the use of CdS as a sensitiser to ZnO NRs.

Optical band gaps for both ZnO NRs and ZnO NRs/CdS core shell thin films were derived using Tauc's equation (2)

$$(\alpha h\nu)^2 = A\left(h\nu - E_g\right), \tag{2}$$

where $h\nu$ is the photon energy, E_g is the optical band gap, A is a constant and α is the absorption coefficient.

Values of optical band gaps for ZnO NRs & ZnO NRs/CdS core shell were found to be 3.165 and 2.368 eV, respectively (Fig. 7), which agree well with previously reported values in the literature [24–26]. The measurement values also indicate the presence of CdS with ZnO nanostructure.

Fig. 8 shows room temperature PL spectrum of prepared samples at an excitation wavelength of 350 nm. It is observed that the spectrum consists of near-band edge (NBE) as well as deep level emissions. The bare ZnO NRs emit a strong UV luminescence NBE peak at 387 nm. This NBE emission is attributed to radiative recombination of free excitons [7, 27]. Another luminescence peak

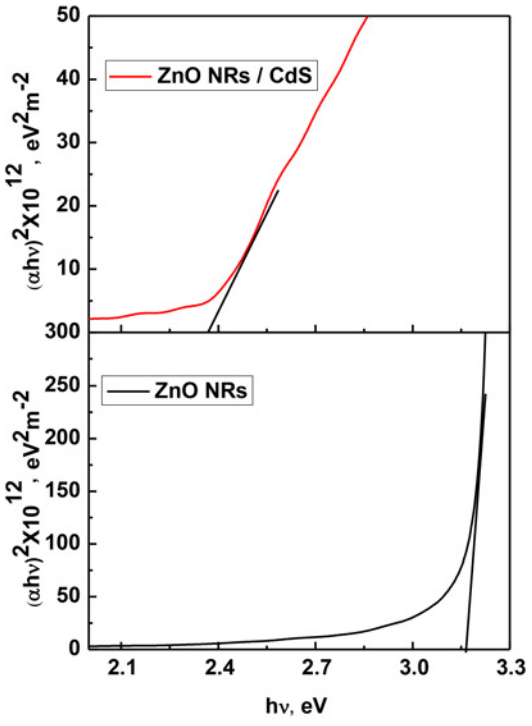

Fig. 7 *Optical bandgap determination of bare ZnO NRs and ZnO NRs/CdS core shell nanostructure*

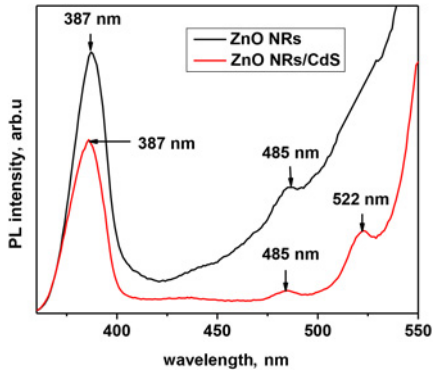

Fig. 8 *PL spectra of ZnO NRs and ZnO NRs/CdS thin films*

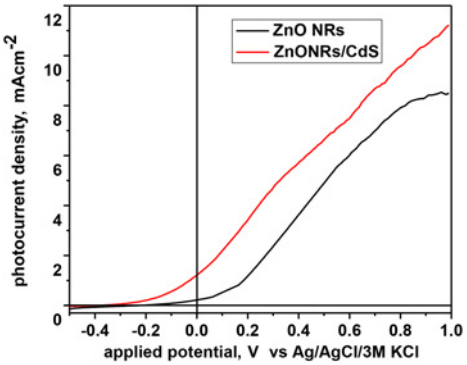

Fig. 10 *Change in photocurrent density as a function of applied bias potential*

appearing at 485 nm is responsible for blue emission and it originates due to the electron transition from the shallow donor level (ionised oxygen vacancies/zinc interstitials) to the top of the valence band [28]. The emission (NBE as well as a deep level) from ZnO NRs is greatly reduced in case of ZnO NRs covered with CdS shell layer. Reduction in PL intensity is partly due to the absorption of incident light and emissions from ZnO NRs by CdS shell layers. The band alignment in ZnO NRs/CdS core shell structures facilitates spatial separation of charges, which efficiently suppresses the radiative recombination of photo-generated electrons and holes and resulted in PL quenching [7]. The spatial charge separation and resultant PL quenching should be the major factor for PL intensity reduction in the measured PL spectrum of ZnO NRs/CdS. The green emission peak centred at 522 nm in PL of ZnO NRs/CdS is attributed to NBE emission associated with the radiative recombination of free excitons in CdS at room temperature [7].

3.3 PEC analysis: PEC activity of the ZnO NRs and ZnO NRs/CdS core shell photoanode was determined using chronoamperometry (Fig. 9) and LSV (Fig. 10) techniques. The LSV measurements were conducted at −0.5 to 1.0 V versus Ag/AgCl/3 M KCl in 0.5 M Na_2SO_4 electrolyte. The photocurrent density versus time graph of bare ZnO NRs and ZnO NRs/CdS core shell films in 0.5 M Na_2SO_4 solution was recorded at zero bias potential versus Ag/AgCl/3 M KCl. As shown in Figs. 9 and 10, photocurrent density of ZnO NRs/CdS core shell photoanode is much higher than bare ZnO NRs photoanodes. The maximum photocurrent density observed for ZnO NRs/CdS core shell photoanodes was 1.75 mA cm^{-2} at zero bias potential, which is similar in value reported by Yang *et al.* [7] (1.7 mA cm^{-2} at 0 V versus saturated calomel electrode (SCE)) and higher than the reported value of Iyenger *et al.* [15] (0.21 $mAcm^{-2}$ versus reversible hydrogen electrode (RHE)) under identical illumination conditions. Fig. 8 shows photocurrent density of ZnO NRs/CdS core shell photoanode has a transient increase when the light is turned on and a fast decrease when the light is turned off, indicating that the ZnO NRs/CdS core shell photoanodes have a fast response speed. A large effective surface area of ZnO NR structure in close proximity with CdS nanoparticles layer results in fast transport of photo-generated electrons and holes.

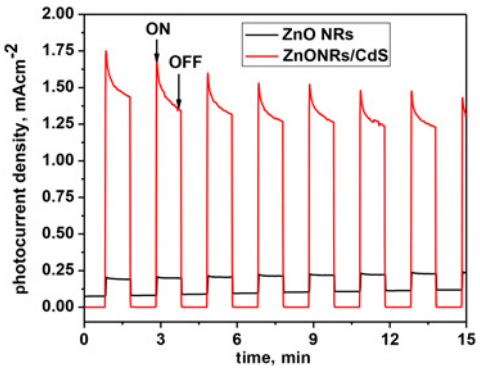

Fig. 9 *Change in photocurrent density as a function of time*

The band gap diagram of ZnO NRs/CdS composite is shown in Fig. 11. Due to illumination, direct photo excitation occurs that lead to the generation of electron–hole pair. The electrons generated in CdS coating by visible light excitation will transfer in the conduction band of the ZnO NRs and subsequently to the FTO and to Pt counter electrode to generate H_2 through reduction of protons, while the photo-generated holes in the CdS layer would react with water to generate O_2 [6–8].

The optical to chemical energy conversion efficiency can be calculated using (3) [6, 7]

$$\eta(\%) = \frac{j_{ph}\left(1.23 - V_{RHE}\right) \times 100\%}{TP_0}. \tag{3}$$

Here j_{ph} is the photocurrent density (mA cm^{-2}), P_0 is the incident light intensity (100 mW cm^{-2}), T is the transmittance of light incident on photo electrode (0.8 in this study) and V_{RHE} is the applied bias potential versus RHE. V_{RHE} is related to the applied potential versus Ag/AgCl/3 M KCl ($V_{Ag/AgCl/3\ M\ KCl}$), according to the Nernst equation (4) [7]

$$V_{RHE} = V_{Ag/AgCl/3\,M\,KCl} + 0.059\,pH + 0.210. \tag{4}$$

The optical to chemical conversion efficiencies (η) of the photoanodes were calculated according to (3). As shown in Fig. 12, optical

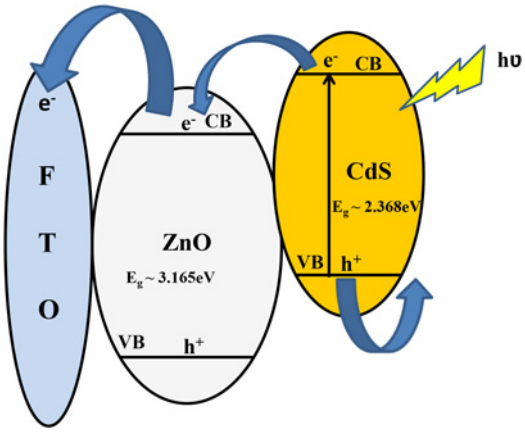

Fig. 11 *Schematic representation of energy levels of the ZnO NRs/CdS core shell structure*

doi: 10.1049/mnl.2018.5700

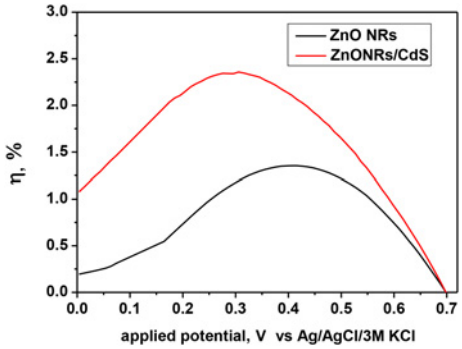

Fig. 12 *Optical-to-chemical conversion efficiency of the bare ZnO NRs and ZnO NRs/CdS core shell photoanodes*

to chemical conversion efficiency (η) of 1.07% is obtained at 0 V versus Ag/AgCl/3 M KCl for ZnO NRs/CdS core shell photoanode, compared to 0.19% for the bare ZnO NRs photoanode. The maximum efficiency for ZnO NRs/CdS core shell photoanode is ~2.357% (at 0.305 V versus Ag/AgCl/3 M KCl), which is about 1.75 times higher than that of bare ZnO NRs (1.35% at 0.406 V versus Ag/AgCl/3 M KCl) indicating the enhanced PEC activity of ZnO NRs/CdS core shell photoanode. The achieved photocurrent conversion efficiency (PCE) in this work is much higher than that reported by Rokade *et al.* [6] (0.29% at 0.5 V versus SCE) and Yang *et al.* [7] (1.35% at 0.17 V versus RHE) under identical illumination conditions.

All these results suggest that the addition of the CdS layer on ZnO NRs' arrays is beneficial for higher light absorption in the visible region. It results in enhancement of interfacial charge transport and separation efficiency of photo-generated charges, which leads to improvement of photocurrent conversion efficiency in water splitting. Besides, the bottom layer of the ZnO NRs/CdS core shell photoanode has a uniform, dense, 1D, long ZnO NRs structure, which facilitates faster and unidirectional electron transport [29, 30].

In most of the previous works, CdS was deposited on to ZnO NRs by conventional solution-based (CBD or Successive Ion Layer Absoption and Reaction (SILAR)) techniques [2, 5, 6] or more complex pulsed laser deposition techniques [7]. In CBD or SILAR techniques, contact between solution and ZnO NRs results in degradation of ZnO NRs. Reduction in the length of the ZnO NRs results in loss of support for the adherent CdS nanocrystals. Also, in conventional solution-based techniques, growth of isolated CdS particle was observed instead of ZnO NRs/CdS core shell structures. In this present work, pH of NCLD precursor solution was kept at ~6.6, which minimised leaching of ZnO NRs. The NCLD technique also enabled selective deposition of CdS nanocrystals on top of ZnO NRs which led to the formation of uniform CdS shell layer preserving ZnO NRs core structure.

4. Conclusion: Vertically aligned uniform 1D ZnO NRs and ZnO NRs/CdS core shell structures have been successfully synthesised on FTO-coated SLG substrate employing cost effective chemical routes and less hazardous NCLD technique. Hexagonal wurtzite 1D structures of the thin films were confirmed by the XRD and FESEM studies. Vis light absorption ability of wide band gap ZnO NRs was enhanced by coating narrow band gap CdS on the surfaces of ZnO NRs. ZnO NRs/CdS core shell showed improved optical band gap, increase in absorption in the Vis region and higher PCE activity. An optical-to-chemical conversion efficiency of 2.357% was achieved for ZnO NRs/CdS core shell photoanode which is about 1.75 times higher than ZnO NRs photoanodes (1.35%).

5. Acknowledgments: Authors are grateful to the support of Director CSIR-CGCRI in carrying out this research work. The cooperation received from AMMCD and Sol-gel Division during this research work is also acknowledged.

6 References

[1] Caruso F.: 'Nanoengineering of particle surfaces', *J. Adv. Mater.*, 2001, **13**, (1), pp. 11–22
[2] Krishnaveni M., Devadason S.: 'Enhancement of the luminescence of ZnO nanorod arrays by SILAR coating with a CdS nano crystalline shell layer', *J. Electron. Mater.*, 2015, **44**, (2), pp. 706–714
[3] Sakthivel S., Neppolian B., Shankar M.V., *ET AL.*: 'Solar photocatalytic degradation of azodye: comparison of photocatalytic efficiency of ZnO and TiO_2', *Sol. Energy Mater. Sol. C*, 2003, **77**, pp. 65–82
[4] Wang M., Ren F., Cai G., *ET AL.*: 'Activating ZnO nano rod photoanodes in visible light by Cu ion implantation', *Nano Res.*, 2014, **7**, pp. 353–364
[5] Qiu X., Que W., Yin X., *ET AL.*: 'ZnO/CdS/CdSe core/double shell nanorod arrays derived by a successive ionic layer adsorption and reaction process for quantum dot-sensitized solar cells', *Semicond. Sci. Technol.*, 2011, **26**, p. 095028
[6] Rokade A., Rondiya S., Date A., *ET AL.*: 'Electrochemical synthesis of core-shell ZnO/CdS nanostructure for photocatalytic water splitting application', *Energy Proc.*, 2017, **110**, pp. 121–127
[7] Yang X., Li H., Zhang W., *ET AL.*: 'High visible photo electrochemical activity of Ag nanoparticle - sandwiched CdS/Ag/ZnO nanorods', *ACS Appl. Mater. Interfaces*, 2017, **9**, pp. 658–667
[8] Li B., Wang Y.: 'Synthesis, microstructure, and photocatalysis of ZnO/CdS nano-heterostructure', *J. Phys. Chem. Solids*, 2011, **72**, (10), pp. 1165–1169
[9] Shen Q., Zhao X., Zhou S., *ET AL.*: 'Zno/CdS hierarchical nanospheres for photo electrochemical sensing of Cu^{2+}', *J. Phys. Chem. C*, 2011, **115**, (36), pp. 17958–17964
[10] Wang X., Liu G., Lu G.Q., *ET AL.*: 'Stable photocatalytic hydrogen evolution from water over ZnO–CdS core–shell nanorods', *Int. J. Hydrogen Energy*, 2010, **35**, (15), pp. 8199–8205
[11] Barpuzary D., Khan Z., Vinothkumar N., *ET AL.*: 'Hierarchically grown urchinlike CdS@ZnO and CdS@Al_2O_3 heteroarrays for efficient visible-light-driven photocatalytic hydrogen generation', *J. Phys. Chem. C*, 2012, **116**, (1), pp. 150–156
[12] Wang X., Yin L., Liu G., *ET AL.*: 'Polar interface-induced improvement in high photocatalytic hydrogen evolution over ZnO–CdS heterostructures', *Energy Environ. Sci.*, 2011, **4**, (10), pp. 3976–3979
[13] Khanchandani S., Kundu S., Patra A., *ET AL.*: 'Shell thickness dependent photocatalytic properties of ZnO/CdS core-shell nanorods', *J. Phys. Chem. C*, 2012, **116**, (44), pp. 23653–23662
[14] Tak Y., Hong S.J., Lee J.S., *ET AL.*: 'Solution-based synthesis of a CdS nanoparticle/ZnO nanowire heterostructure array', *Cryst. Growth Des.*, 2009, **9**, (6), pp. 2627–2632
[15] Iyengar P., Das C., Balasubramaniam K.R.: 'Photoelectrochemical performance of NiO-coated ZnO–CdS core–shell photoanode', *J. Phys. D, Appl Phys.*, 2017, **50**, p. 10LT01
[16] Dris M.R.M., Sheng C.K., Isa M.I.N., *ET AL.*: 'A study of cadmium sulphide nanoparticles with starch as a capping agent', *Int. J. Technol.*, 2012, **3**, (1), pp. 1–7
[17] McFarland E.W., Tang J.: 'A photovoltaic device structure based on internal electron emission', *Nature*, 2003, **421**, (6923), pp. 616–618
[18] Hotchandani S., Kamat P.V.: 'Charge-transfer processes in coupled semiconductor systems. Photochemistry and photo electrochemistry of the colloidal cadmium sulfide-zinc oxide system', *J. Phys. Chem.*, 1992, **96**, (16), pp. 6834–6839
[19] Chen R., Fan J., Liu C., *ET AL.*: 'Solution-processed one-dimensional ZnO @ CdS heterojunctional toward efficient Cu_2ZnSnS_4 solar cell with inverted structure', *Sci. Rep.*, 2016, **6**, DOI: 10.1038/srep35300
[20] Biswas I., Majumder M., Roy(Kundu) P., *ET AL.*: 'Nanostructured ZnO thin film with improved optical and electrochemical properties prepared by hydrothermal electrochemical deposition technique', *Micro Nano Lett.*, 2016, **11**, (7), pp. 351–355
[21] Lee D., Yong K.: 'Superstrate $CuInS_2$ photovoltaics with enhanced performance using a CdS/ZnO nanorod array', *ACS Appl. Mater Inter.*, 2012, **4**, pp. 6758–6765
[22] Singh P., Kumar A., Deepak D.K., *ET AL.*: 'Zno nanocrystalline powder synthesized by ultrasonic mist-chemical vapour deposition', *Opt. Mater.*, 2008, **30**, pp. 1316–1322

[23] Romero M., Henriquez R., Dalchiele E.A.: 'Electrochemical deposition of ZnO nanorod arrays onto a ZnO seed layer: nucleation and growth mechanism', *Int. J. Electrochem. Sci.*, 2016, **11**, pp. 8588–8598
[24] Kathalingam A., Kim M.R., Chae Y.S., *ET AL.*: 'Studies on electrochemically deposited ZnO thin films', *J. Korean Phys. Soc.*, 2009, **55/6**, pp. 2476–2481
[25] Fan D., Thomas P.J., O'Brien P.: 'Deposition of CdS and ZnS thin films at the water/toluene interface', *J. Mater Chem.*, 2007, **17**, pp. 1381–1386
[26] Ouachtari F., Rmili A., Elidrissi S.E.B., *ET AL.*: 'Influence of both temperature, deposition time and [S]/[Cd] ratio on the structure, surface morphology, chemical composition and optical properties of CdS thin films elaborated by chemical bath deposition', *J Mod. Phys.*, 2011, **2**, pp. 1073–1082
[27] Vanheusden K., Warren W.L., Seager C.H., *ET AL.*: 'Mechanisms behind green photoluminescence in ZnO phosphor powders', *J. Appl. Phys.*, 1996, **79**, pp. 7983–7990
[28] Xue Z.Y., Zhang D.H., Wang Q.P., *ET AL.*: 'The blue photoluminescence emitted from ZnO films deposited on glass substrate by rf magnetron sputtering', *Appl. Surf. Sci.*, 2002, **195**, pp. 126–129
[29] Benkstein K.D., Kopidakis N., van de Lagemaat J., *ET AL.*: 'Influence of the percolation network geometry on electron transport in dye sensitized titanium dioxide solar cells', *J. Phys. Chem. B*, 2003, **107**, pp. 7759–7767
[30] Frank A.J., Kopidakis N., van de Lagemaat J.: 'Electrons in nanostructured TiO_2 solar cells: transport, recombination and photovoltaic properties', *J. Coord. Chem. Rev.*, 2004, **248**, pp. 1165–1179

doi: 10.1049/mnl.2018.5700